Available online at www.sciencedirect.com
ScienceDirect
Acta Materialia 58 (2010) 6495–6503
Acta MATERIALIA
www.elsevier.com/locate/actamat

Design and fabrication of compositionally graded inorganic oxide thin films: Mechanical, optical and permeation characteristics

Y.-H. Choi [a], X. Bulliard [a], A. Benayad [a], Y. Leterrier [b], J.-A.E. Månson [b], K.-H. Lee [a], D. Choi [c,*], J.-J. Park [a,**], J. Kim [a]

[a] Samsung Advanced Institute of Technology, Yongin, Gyeonggi 446-712, Republic of Korea
[b] Laboratoire de Technologie des Composites et Polymères (LTC), Ecole Polytechnique Fédérale de Lausanne (EPFL), Station 12, CH-1015 Lausanne, Switzerland
[c] Department of Mechanical Engineering, College of Engineering, Kyung Hee University, Yongin, Gyeonggi 446-701, Republic of Korea

Received 21 June 2010; accepted 12 August 2010

Abstract

Different types of inorganic oxide films composed of a chemical composition gradient single layer were designed, fabricated and characterized. Compositionally graded thin films were created by power-controlled co-sputtering of alumina (Al_2O_3) and silica (SiO_2) at room temperature, allowing the structural design of the film to be tailored at the nanometer scale. Two distinct graded thin films were fabricated: one with a compositionally asymmetric structure consisting of a SiO_2-rich bottom interface and a Al_2O_3-rich top surface, and the other with a compositionally balanced sandwich structure consisting of both the top surface and bottom interface rich in SiO_2 and a core rich in Al_2O_3 (referred to as SGS for 'sandwich graded structure'). Smoothly graded thin films without interfacial boundaries were verified by Auger electron spectroscopy profiles. X-ray photoelectron spectroscopy demonstrated that the Al_2O_3/SiO_2 graded structures consisted of Si–O and Al–O bonds, as well as Al–O–Si bonds in the transition layer. Neat Al_2O_3 or SiO_2 and their graded ones were all investigated for their mechanical, optical and permeation properties. A SGS thin film presented the best mechanical stability (i.e., about three times improved film toughness of a neat Al_2O_3 single layer), demonstrating that balanced internal stresses and alternating bonding structures, achieved via a graded structure without interfaces, are crucial for enhancing mechanical stability. Furthermore, neat and graded thin films exhibited the similar level of optical transmittance and the permeation properties for the graded films were well matched with the behaviors of mechanical stability.

Keywords: Functionally graded materials; Thin films; Interface structure; Sputtering; Toughness

1. Introduction

Inorganic oxides are used in a variety of electronic, biological and structural devices owing to their unique properties such as optical transparency, high thermal/mechanical resistivity and high electrical properties, depending on the material [1–3]. Examples are insulators in thin film transistors [4], optical spacers or electron/hole blocking/transporting layers in photovoltaic systems [5,6], encapsulating gas barriers for organic electronics [7,8] and dielectric material in plasmonic molecular sensors [9,10]. Recently, as many devices have been developed with light, thin and even flexible characteristics, the need for thin film types of functional inorganic oxides is rapidly increasing, and the mechanical stability of inorganic thin films is inevitably becoming important for applications, particularly in flexible electronics [11–14].

The intrinsic mechanical strength of inorganic oxides is extremely high, even though they are brittle. However,

* Corresponding author. Tel.: +82 31 201 3320; fax: +82 31 202 8106.
** Corresponding author. Tel.: +82 31 280 6775; fax: +82 31 280 6728.
E-mail addresses: dchoi@khu.ac.kr (D. Choi), jongjin00.park@samsung.com (J.-J. Park).

1359-6454/$36.00 © 2010 Acta Materialia Inc. Published by Elsevier Ltd. All rights reserved.
doi:10.1016/j.actamat.2010.08.011

depending on the fabrication process, the extrinsic properties of inorganic oxide thin films are significantly changed by defects such as pinholes or cracks introduced during manufacture. In general, inorganic oxide thin films are fabricated on a substrate by sputtering, chemical vapor deposition (CVD), atomic layer deposition (ALD), laser ablation and sol–gel coating [15–19]. Furthermore, self-supporting ultrathin films have been developed by several preparative techniques, such as solvent casting, self-assembly ABA triblock copolymer and cross-linking of Langmuir–Blodgett [20–22]. Among these fabrication methods, ALD provides high-density and high-quality (i.e., low defects) thin films based on the layer-by-layer deposition process at atomic scale, but the deposition method is limited by the restricted size and a high-cost, low-throughput and slightly high-temperature fabrication process. However, radio-frequency (RF) magnetron sputtering can provide a cost-effective, high-throughput and relatively low temperature process with large area scalability and co-sputtering capability, but the thin films deposited from vapor usually have many defects, thus severely degrading the physical properties of the films. Since those defects also control the toughness and the related strain to failure of the layer, it is of vital importance to minimize the defects to achieve uniform and macroscopic robust high-quality thin films through a high-throughput process on a large area [2].

Functionally graded materials (FGM) [23–25] offer a way to improve the mechanical resistance of inorganic materials. As an example, Hertzian cracks induced by indentation can be drastically reduced using graded materials [26]. The benefit is due to the increase in elastic modulus with increasing depth from the top surface, reducing the maximum principal tensile stresses in the bulk material of the FGM. A similar approach has recently been used to create films with a composition gradient across the thickness in an organic/inorganic hybrid structure [19]. The main objective was to prevent delamination (i.e., improving the adhesion property) between the film layer and a polymer substrate by creating a smooth transition in mechanical properties and reducing stress discontinuities across the interface. Disadvantages of previous techniques for FGM are, however, the thickness of the final film structure, greater than a few micrometers, and the complex, high-temperature solution-based fabrication processes involved, such as the annealed diffusion method, electrochemical deposition, metal–organic CVD and sol–gel coating.

This work exploits the graded approach in a simpler way, to create high-quality single layer thin films at low temperature. Inorganic oxide thin films with thickness <200 nm, and composition gradient controlled at the nanometer scale across their thickness, are achieved using RF magnetron co-sputtering of Al_2O_3 and SiO_2. Differing graded thin films are investigated, with attention paid to their mechanical, optical and permeation properties, and compared with those of non-graded neat single layers. A crucial point is the absence of sharp interfaces across the thickness, with a smooth chemical transition from the two distinct materials, as confirmed by the presence of Al–O–Si bonds in the film. This approach offers great flexibility for thin film design at a nanometer scale, with the capability to choose the composition of materials in contact with the substrate as well as the core composition of the film, so as to provide optimal interfacial control and mechanical integrity.

2. Experimental

2.1. Power-controlled co-sputtering for a graded structure

A modified RF magnetron co-sputtering machine (INFOVION Inc.) in which the cathode guns are computer-controlled was used to fabricate thin films with a graded structure. Programmed automatic control for the cathode guns was realized in the range 0–600 W for both Al_2O_3 and SiO_2 over a time of 10 min. It was arranged that one cathode gun has an Al_2O_3 target (99.99% purity) and the other has a SiO_2 target (99.99% purity). Single layered graded structures were then fabricated on flexible polymer substrates such as polyethylene terephthalate (PET) and polyether sulfone (PES), and on a Si(1 0 0) substrate by non-reactive RF magnetron co-sputtering processes at a low temperature <100 °C in Ar at a flow rate of 100 sccm. The working pressure was 5 mtorr and the substrate was rotated at 10 rpm during deposition. The reference samples of pure (meaning 99.99%) Al_2O_3 and SiO_2 were prepared by non-reactive RF magnetron co-sputtering with power ratios of 600:0 W (for Al_2O_3) and 0:600 W (for SiO_2).

2.2. Structural characterization

The microstructures of the films were investigated in cross-section by transmission electron microscopy (TEM; Tecnai f20st FEI). Samples for TEM were prepared by mechanical pre-thinning and Ar ion milling at 4 keV. Phase analysis of films was performed by X-ray diffraction (XRD) using Cu K_α radiation ($\lambda = 0.154$ nm). The chemical composition of the graded structures was characterized by X-ray photoelectron spectroscopy (XPS; Physical Electronics Quantum 2000 scanning ESCA microprobe) using focused monochromatized Al K_α radiation (1486.6 eV; the diameter of the irradiated area was 100 μm). The spectrometer, with energy resolution 0.3 eV, was calibrated using photoemission lines of gold (Au 4f7/2 = 84.0 eV, with reference to Fermi level). Depth–composition profiles of the graded Al_2O_3/SiO_2 structure were performed using Auger electron spectroscopy (AES; Microlab 350), with a 10 keV electron-beam and 1 keV Ar^+ at an angle of incidence of 30° for depth sputtering into a 1 × 1 mm area. Optical transmission spectra of the graded films were obtained using a Varian Cary 5000 UV–Vis spectrometer. The refractive indexes of the homogeneously mixed films were determined by polarizer rotating ellipsometer (Elli-SE(UV)-FM9) in the optical range 238–1033 nm.

2.3. Fragmentation tests

Fragmentation tests were undertaken to determine the cohesive and adhesive properties of the thin films on the polymer substrates. The evolution of crack patterns in the brittle coating is monitored in situ as a function of the uniaxial tensile load applied to the substrate, using a microscope. A tensile load was applied to rectangular film specimens ($50 \times 5\ mm^2$) with a computer-controlled Minimat unit (Rheometric Systems), using a stepper motor for crosshead displacement to an accuracy of within 1 μm. The tensile unit was mounted under an optical microscope (Olympus BX60) equipped with a charge-coupled device camera (Soft Imaging Systems ColorView II) for non-contact video extensometry of specimen strain, with accuracy better than 10^{-4} in the strain values [27]. This method eliminated problems with frame compliance. Cracking of the coatings was analyzed at increasing strain levels via the crack density (CD), calculated from the mean number of cracks N_i, counted on $k = 7$ micrographs of width W, at strain ε, as $CD = (1+\varepsilon)\sum_{i=1}^{k} N_i/kW$. The factor $(1+\varepsilon)$ is a correction for crack opening. The crack onset strain (COS), corresponding to the onset of unstable propagation of the first crack, was obtained by extrapolation of the CD data to $CD = 0$.

2.4. Measurement of permeation property

To investigate the water vapor transmission rate (WVTR) characteristic for the graded structures and the references, thin films were prepared on 100-μm-thick PET substrates. The WVTR was measured for films with an active area of 50 cm^2, at 37.8 °C and 100% relative humidity, using a MOCON AQUATRAN® Model 1, with a reliable detectable range of 0.0001–60 g m^{-2} day^{-1}.

3. Results and discussion

3.1. Design of chemical composition graded structures

RF magnetron co-sputtering equipment was designed, with SiO_2 and Al_2O_3 targets, in which the power of each cathode gun was regulated independently to control the deposition of inorganic layers with graded mixed composition. The power was matched so as to create a composition gradient, using a succession of stepwise stages of ~10 min, with a power intensity varying between 0 and 600 W (see Fig. 1a). To verify the progressive change in composition between deposition stages, XPS was conducted on a sample of graded structure with the bottom interface composed entirely of SiO_2 and the top surface entirely of Al_2O_3. Fig. 1b shows XPS survey spectra and highlights the monotonic decrease in the intensity of Si-related peaks (Si 2s and Si 2p core peaks) and the increase in Al-related peaks (Al 2s and Al 2p core peaks) without significant change in the O 1s peak intensity. This observation confirms that this technique is capable of making single layered inorganic thin films with a chemical composition that is smoothly graded. The film with a variety of graded structures is easily realized through modulation of the power ratio of each cathode gun during co-sputtering.

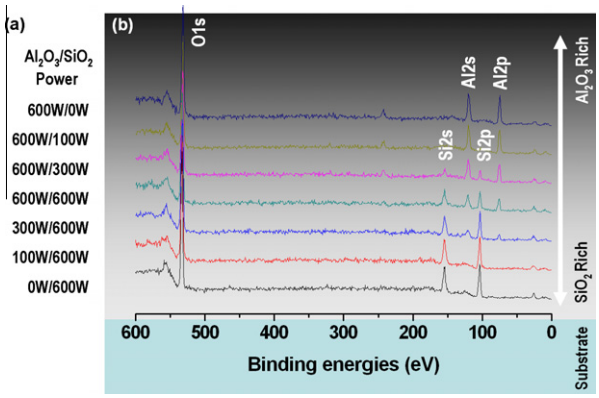

Fig. 1. Design of a chemical composition graded nanoarchitecture by power-controlled co-sputtering. (a) Power ratio of each cathode gun for Al_2O_3 and SiO_2 targets, respectively. The power ratio for the guns was automatically controlled every 10 min. (b) Typical XPS spectra for Si-related peaks (Si 2s and Si 2p core peaks) and Al-related peaks (Al 2s and Al 2p core peaks).

Using this method for graded structures, the authors designed thin films with a graded structure at nanometer scale. Two distinct graded architectures were then designed: one with a continuous composition change from a SiO_2-rich bottom interface to an Al_2O_3-rich top surface (referred to as AGS for 'asymmetric graded structure'; Fig. 2a) and the other with both the top surface and bottom interface rich in SiO_2 and a core rich in Al_2O_3 (referred to as SGS; Fig. 2b). In these structures, SiO_2 was coated on the polymer substrate in order to reduce internal stresses and improve adhesion, since Al_2O_3 has a high tensile modulus but is brittle, and SiO_2 is tougher than Al_2O_3.

It is important to check that the deposition technique did not induce any further interface within the single layer, while modifying the chemical composition by tuning the power of each cathode. Fig. 2c and d shows TEM images of the graded structures on a Si wafer. No interfacial boundaries in the graded structures were visible. The high-resolution TEM (HR-TEM) images (right top and bottom images of each TEM image) at positions I and II of the TEM images clearly confirm the absence of boundaries in the graded structures. Furthermore, all the graded films are of amorphous structure confirmed by the TEM images and the XRD results. (No distinct diffraction peaks were checked; data not shown.) AES was then used to study the concentration depth-profiles of the graded samples. Fig. 2e shows a linear decrease in the Si concentration from the bottom interface to the top surface, whereas Al increases linearly in the continuous graded film. The atomic concentration of oxygen was constant throughout the layer. The profiles are accurately linear without marked steps, confirming the regularity of the change in concentration with thickness. Fig. 2f shows the profile for the SGS.

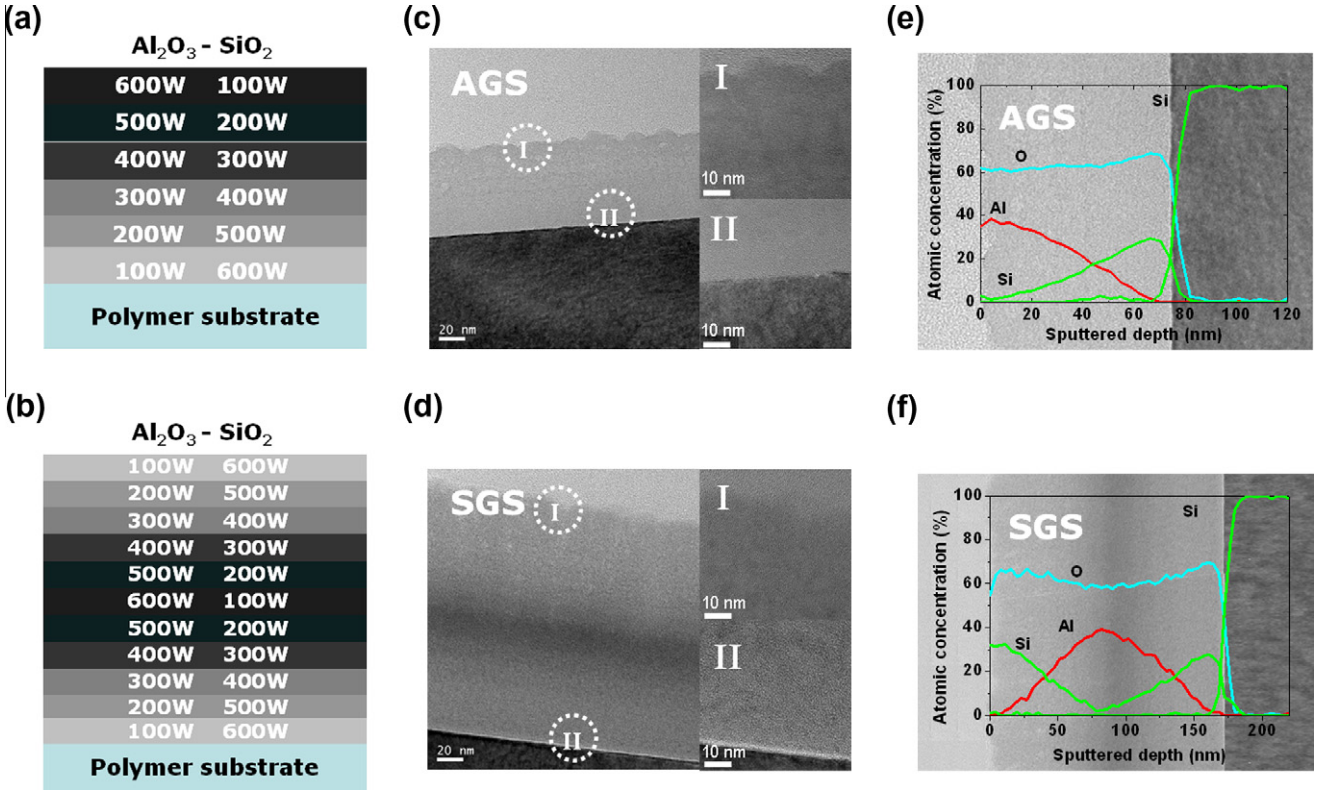

Fig. 2. Characterization of compositionally graded structures. Fabrication processes for two distinct graded structures: (a) AGS and (b) SGS; (c) and (d) TEM images of the graded structures which demonstrate no sharp interfacial boundaries in the graded structures. This smoothness was further confirmed from HR-TEM images at regions I and II of the images. AES depth-profiles for (e) AGS and (f) SGS according to the film thickness (i.e., sputtered depth), showing the continuously graded concentration of each inorganic material.

Again the profiles were smooth, with regular convex or concave curvatures for Si and Al, respectively.

3.2. Characterization of bond type

The results obtained by TEM and AES show that the single graded layers have no abrupt interfaces, with a smooth change in concentration. XPS was then used to analyze the nature of chemical bonding in the samples, in particular the possibility of inter-mixing. The XPS studies focused on the core peaks of simple mixtures (i.e., non-graded) of Al_2O_3/SiO_2 prepared by changing the power ratio applied to the Al_2O_3 and SiO_2 targets. Two pure Al_2O_3 and SiO_2 films were also prepared and used as references. Analysis of core peak binding energies in association with their chemical shifts allowed us to determine the local chemical environments of Al and Si elements.

Fig. 3 shows high-resolution XPS Al 2p, Si 2p and O 1s core-level spectra of Al_2O_3/SiO_2 mixture films for differing values of the co-sputtering power ratio. The XPS Si 2p and Al 2p core-level spectra corresponding to the pure SiO_2 and Al_2O_3 thin films are at 103.6 and 74.6 eV (see Table 1 and Fig. 3), associated with +4 and +3 formal degrees for Si and Al, and corresponding to Si–O and Al–O bonds, respectively. The O 1s core peaks of the SiO_2 and Al_2O_3 films were observed at 532.7 and 531.2 eV, corresponding to O^{2-} ions in the Si–O and Al–O local environment, respectively. The XPS Al 2p and Si 2p core level peaks for the Al_2O_3/SiO_2 mixture layer, deposited at the power ratio 300:600 W, are positioned at 76.1 and 103.6 eV, respectively, and are attributed to the presence of suboxide AlO_x in the strongly covalent SiO_2 network. This result indicates that Si–O–Al bonds are incorporated in the Si–O network. The Al 2p chemical shift toward lower binding energy (75.6 eV) was more pronounced for the Al_2O_3/SiO_2 layers deposited at 600:300 W, implying a change in film composition with increasing Al_2O_3 content, from the Si–O bond type to the Si–O–Al bond type. Further addition of Al_2O_3 (600:100 W for Al_2O_3/SiO_2) caused the Al 2p, Si 2p, and O 1s core peaks to shift to lower binding energies, indicating a change from Si–O–Al bond type to the predominant Al–O bond in Al_2O_3.

Also, a clear change in the full width at half maximum (FWHM) was observed when the power ratio was ~1:1 (i.e., ~600:600 W). This change indicates the presence of a disordered system and/or the existence of distinct local environments for Al, Si and O atoms (i.e., Si–O, Al–O and Al–O–Si bonds). These results show that a continuous change in the local chemical bond type occurs as the applied power ratio is changed.

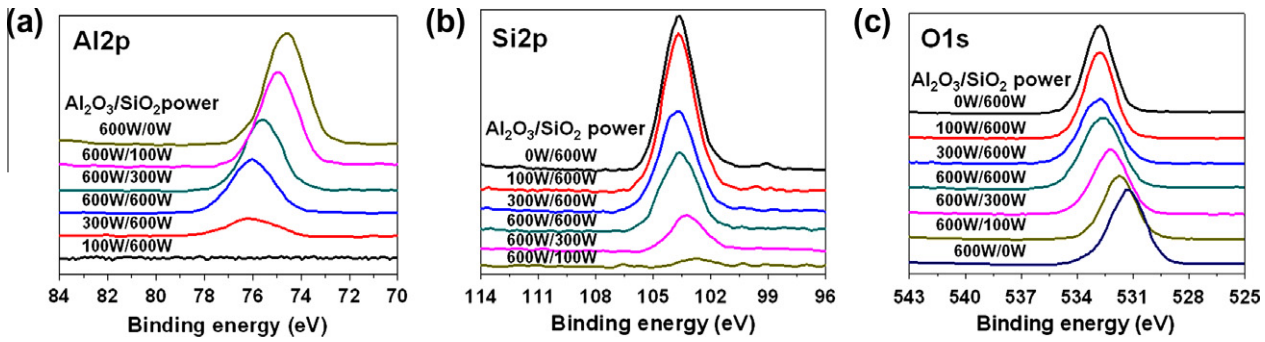

Fig. 3. Core level XPS spectra of (a) Al 2p, (b) Si 2p and (c) O 1s in Al_2O_3/SiO_2 mixture layers with differing power ratios. Compared with the binding energy peaks for the pure Al_2O_3 and SiO_2 (i.e., at 600:0 W and 0:600 W data), the XPS spectra of the mixtures shows a shift in the peak with differing power ratio. Furthermore, when the power ratio was approximately 1:1, the peaks were broad.

Table 1
Si2p, Al2p and O1s binding energies in differing Al_2O_3/SiO_2 mixture films; the atomic percentages from the XPS quantitative analyses of different elements are indicated in square brackets, and FWHM values in parentheses.

Al_2O_3/SiO_2 power ratio (W:W)	Si 2p (eV) (FWHM) [at.%]	Al 2p (eV) (FWHM) [at.%]	O 1s (eV) (FWHM) [at.%]
0/600 (SiO_2)	103.6 (1.9) [35]	*** (***) [***]	532.7 (1.8) [65]
100/600	103.6 (1.9) [35]	*** (***) [***]	532.7 (1.8) [65]
300/600	103.6 (2.1) [27]	76.1 (2.3) [7]	532.6 (2.3) [66]
600/600	103.6 (2.2) [17]	76.0 (2.0) [17]	532.5 (2.4) [66]
600/300	103.2 (2.1) [10]	75.6 (1.8) [24]	532.2 (2.2) [66]
600/100	102.7 (2.1) [2]	74.9 (1.8) [33]	531.7 (2.2) [65]
600/0 (Al_2O_3)	N/A	74.6 (1.9) [34]	531.2 (2.2) [66]

3.3. Mechanical analysis of non-graded and graded films

Fragmentation tests [28–31] were undertaken to verify the advantages of creating a graded architecture by examining the mechanical integrity of the layers, using a PES substrate. The elastic properties of the polymer (Young's modulus 2.5 GPa, Poisson's ratio 0.4) and of the Al_2O_3 and SiO_2 layers were taken from the literature, and values for the composite layers were calculated using the rule of mixture. The cohesive and adhesive properties of the layers calculated from the fragmentation data are reported in Table 2, together with the elastic data.

3.3.1. Cohesive properties of oxide layers

Fig. 4 shows the early fragmentation stages of the layers investigated, plotting the density of tensile cracks (CD) against the strain ε. The experimental data were fitted by the equation:

$$CD(\varepsilon) = CD_{sat}(1 - \exp\{-A(\varepsilon - \varepsilon_1)\}) \quad (1)$$

where CD_{sat} represents the CD at saturation of the fragmentation process, A is an adjustable factor which reflects the cracking rate (and is related to parameters such as the coating Weibull modulus) [30], and ε_1 is the COS. The COS was used to estimate the critical radius (R_{crit}) at which cracks are initiated in the bending mode:

Table 2
Elastic, cohesive and adhesive properties of layers on PES.

Coating composition	Thickness h_c (nm)	Elastic properties				Cohesive properties				Adhesive properties	
		Modulus E_c (GPa)	Poisson's ratio (ν_c)	Dundurs parameter (α)	ERR function (g)	COS	Critical radius (mm)	Weibull modulus (m)	Toughness G_c (J m^{-2})	CD_{sat} (mm^{-1})	IFSS (MPa)
Al_2O_3	100	200	0.2	0.972	12.6	0.0056	17.7	3.50	12.1	135	45.0
Al_2O_3	140	200	0.2	0.972	12.6	0.0042	23.8	3.54	9.4	–	–
Al_2O_3	200	200	0.2	0.972	12.6	0.0038	26.3	2.42	11.0	–	–
SiO_2	100	80	0.2	0.931	7.1	0.0099	10.1	–	8.4	–	–
Mixed Al_2O_3–SiO_2	100	140	0.2	0.960	10.3	0.0099	10.1	–	21.4	–	–
AGS	140	140	0.2	0.960	10.3	0.0085	11.8	–	21.9	–	–
SGS	140	140	0.2	0.960	10.3	0.0096	10.4	6.18	28.0	227	97.0

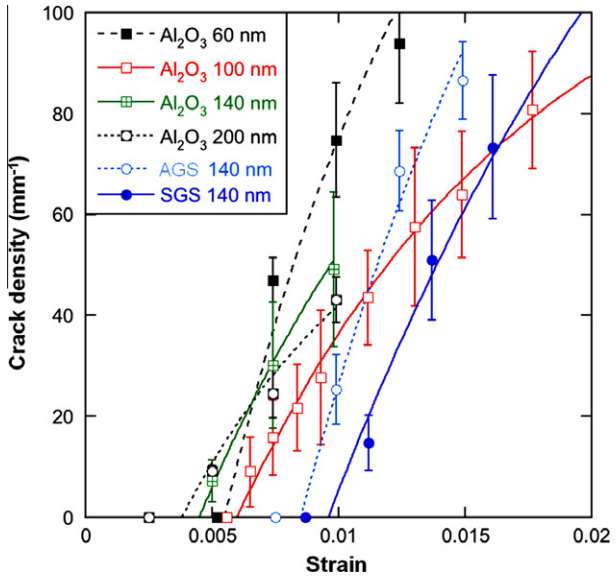

Fig. 4. Density of tensile cracks of inorganic oxide layers on a PES substrate vs. strain.

$$R_{crit} = h_t/(2\varepsilon_1) \quad (2)$$

where $h_t = h_s + h_c$ is the total thickness of the coated substrate, and h_s and h_c are the thicknesses of the substrate and the coat layer, respectively.

The COS of the Al_2O_3 layers decreased from 0.56% to 0.38% as the coating thickness increased from 100 nm to 200 nm. These COS values scale inversely with the square root of the layer thickness, as predicted by linear elastic fracture mechanics. The corresponding critical radius, calculated using Eq. (2), increased from 18 mm to 26 mm. This means that the increasing thickness for an inorganic layer generates lower mechanical flexibility. The Weibull modulus of the layers, which characterizes their defect structure, was also derived from the early fragmentation stages using the approach set out in Ref. [30], and was found to be close to three for the alumina layers. The COS is determined by the energy released during the fracture event, which depends on the layer toughness, layer thickness and the layer/substrate elastic contrast. The toughness of the layers was calculated by assuming that it is equal to the energy release rate (ERR) at COS, using the approach detailed in Refs. [32,33]:

$$G_{ss} = \frac{\pi}{2}\bar{E}_c\varepsilon_1^2 g(\alpha,\beta) \quad (3)$$

where $\bar{E}_c = E_c/(1-\nu_c^2)$ is the plane strain modulus of the layer (E_c and ν_c are the Young's modulus and Poisson's ratio of the layers), and $g(\alpha, \beta)$ is a function of the Dundurs parameters α and β, which describe the elastic mismatch of the layer/substrate system. For plane strain problems, $\alpha = (\bar{E}_c - \bar{E}_s)/(\bar{E}_c + \bar{E}_s)$, where $\bar{E}_s = E_s/(1-\nu_s^2)$ is the plane strain modulus of the substrate (E_s and ν_s are the Young's modulus and Poisson's ratio of the substrate). The ERR function g depends mainly on the parameter α; the present work used $\beta = \alpha/4$ [32]. The Dundurs parameter α and the layer toughness are set out in Table 2. The toughness is close to 10 J m^{-2} for the Al_2O_3 layers.

The COS of a 100-nm-thick SiO_2 layer which was also deposited on the PES substrate was close to 1%, corresponding to a critical radius of 10 mm. The corresponding fracture toughness was 8.4 J m^{-2}, which is slightly less than that of the Al_2O_3 layers. The improved COS and critical radius of the SiO_2 layer over the Al_2O_3 are therefore due primarily to reduced elastic contrast ($g(SiO_2) = 7.1 < g(Al_2O_3) = 12.6$), SiO_2 being less stiff than Al_2O_3. To determine the effect of simple mixing (homogeneous composition without gradient), a layer of thickness 100 nm prepared by co-deposition at 600:600 W of Al_2O_3 and SiO_2 was tested. Mixing of these two components (i.e., simple mixtures) led to a COS similar to that of pure SiO_2. Blending was therefore particularly effective in improving the mechanical resistance of the more brittle Al_2O_3 layer. Interestingly, the fracture toughness of this mixed composition was 21.4 J m^{-2}, twice as high as that of the plain Al_2O_3 layers. This result is taken to be related to the nature of the bonding in the mixture. As shown by XPS measurements, the blend contained a certain amount of Al–O–Si bonding, whose valence and character (covalent or ionic) is different from each of the two pure materials (SiO_2 and Al_2O_3). Since the cohesive properties of a material are related to the nature of its chemical bonds, substitution of Al–O–Al bonds by Al–O–Si bonds is responsible for the improvement in toughness and hence of COS. A detailed and systematic analysis should be undertaken to confirm this statement, and in particular to clarify the role of possible influent parameters, such as the morphology for example.

The COS of the 140-nm-thick AGS and SGS layers was equal to 0.85% and 0.96%, respectively (Fig. 4 and Table 2). The latter value is almost equal to that of the thinner SiO_2 and Al_2O_3/SiO_2 mixed layers. This was due to the toughness of the SGS, which was found to be the highest of all the materials investigated. The corresponding critical radius was close to 10 mm. Moreover, the Weibull modulus of the SGS layer was twice as high as that of the Al_2O_3 layers, reflecting a narrower defect distribution in the SGS layer. It therefore appears that blending Al_2O_3 with SiO_2 in a controlled and graded manner was the best way to increase the tensile properties of these inorganic layers. The superior mechanical properties of the sandwich graded architectures over alternative materials with similar composition (e.g., the mixed and AGS layers) is due primarily to their specific through-stiffness gradient, in addition to a probable residual stress gradient. Increasing the elastic modulus of the graded layers from the top surface to the core is known to improve the resistance to tensile stresses [34]. This is the case if the concentration gradient is smooth, without any steps or discontinuities, to avoid undue stress concentrations, as confirmed by AES. Furthermore, the presence of Al–O–Si shows an ideal transition from ionic to covalent bonding. Again, this architecture minimized the internal stresses in the film, with

no stress concentration in particular areas of the film. Crack initiation at the surface was reduced further by the presence of higher compressive stresses in the superficial SiO_2 compared with Al_2O_3.

3.3.2. Adhesive properties of oxide layers

Fig. 5 compares the fragmentation process of the 100-nm-thick Al_2O_3 and the 140-nm-thick SGS layers, tested up to strain levels close to the saturation limit. Eq. (1) was used to fit the experimental data; the results are shown in Table 2. The interfacial shear strength (IFSS), which characterizes the adhesion between the inorganic layer and the PES substrate, was derived using the perfectly plastic Kelly–Tyson model [35]:

$$\mathrm{IFSS} = 1.337 h_c \sigma_{\max}(l_c) CD_{sat} \quad (4)$$

where $\sigma_{max}(l_c)$ is the coating strength at saturation, and $l_c = 1.496/CD_{sat}$ is the critical stress transfer length [28,30]:

$$\sigma_{\max}(l_c) = \sigma_0 (l_c/l_0)^{-1/m} \Gamma(1 + 1/m) \quad (5)$$

Here σ_0 and m denote the Weibull scale factor and modulus, respectively, and l_0 is a normalization length taken equal to 1 μm. The IFSS of the Al_2O_3 layer on the PES substrate was 45.0 MPa, which compares with the shear stress at yield τ_Y of the PES substrate estimated at 46 MPa from the tensile strength of the polymer σ_Y, using the Von Mises criterion $\tau_Y = \sigma_Y/\sqrt{3}$. This reflects the good adhesion of the Al_2O_3 layer on PES, presumably due to the formation of covalent bonds between the two materials [36]. The IFSS of the SGS layer on the PES substrate was much higher, at 97.0 MPa. This value, considerably greater than the shear stress at yield τ_Y of the PES substrate, implies that the interface was able to strain harden. This again reflects the creation of chemical bonds during the deposition of the first SiO_2 layer. Based on the cohesive and adhesive characterizations of inorganic films, the sandwich graded geometry, with an Al_2O_3 core layer surrounded by two SiO_2-rich layers at the top and bottom of the film, gave the best performance based on both the cohesive and adhesive properties with the PES substrate.

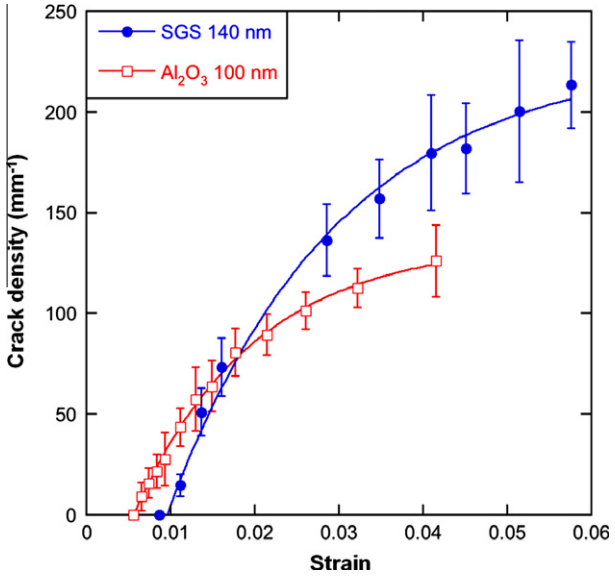

Fig. 5. Density of tensile cracks of Al_2O_3 and SGS layers on a PES substrate vs. strain.

3.4. Optical properties

It was checked whether films with compositionally graded structures preserved high optical transparency of the individual Al_2O_3 or SiO_2 layers. The transmittance of the differing films with a total thickness of 100 nm on a 100-μm-thick PET film is shown in Fig. 6. Except for a slight decrease at wavelengths >500 nm, the optical transmittance of the graded samples remained similar to that of non-graded pure samples. The high transmittance of graded thin films is suitable for a variety of applications in optical electronic devices for which a high transparency is required, so as to minimize the loss of incident light passing through the films.

3.5. Permeation characterizations

The gas barrier properties of the films with their different layer architectures were examined for application to a thin film encapsulation of organic electronics. As a reference sample, the water permeation of single Al_2O_3 layers was first measured as a function of thickness; the results are shown in Fig. 7. The WVTR values decreased with increasing thickness, but reached a saturation value for a thickness just <150 nm. This result confirms that WVTR is not improved indefinitely with increasing thickness, because of the increase in the number of defects. A thickness of 140 nm, corresponding to the best WVTR value for a pure Al_2O_3 single layer, was consequently chosen as reference, and the thickness of all other graded or mixed layers was set at that particular value.

The WVTR of the 140-nm-thick SiO_2 layer was 25% higher (i.e., worse) than that of the reference Al_2O_3. In contrast, for the same thickness, the WVTR of the graded

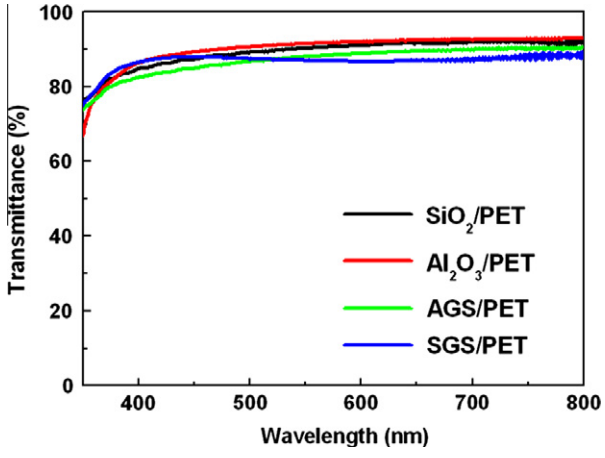

Fig. 6. Transmittance of pure SiO_2, Al_2O_3, and graded structures on PET (100 μm). The thickness of all inorganic single layers is 100 nm.

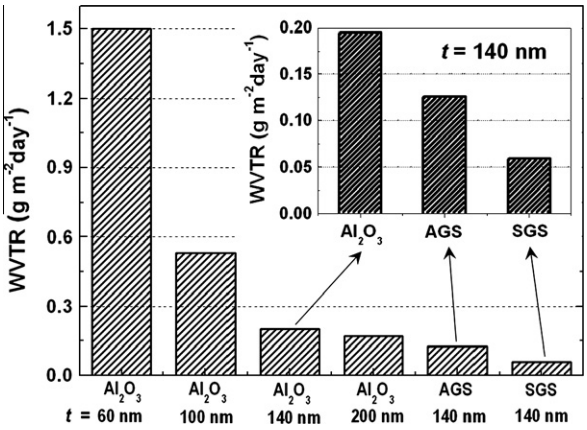

Fig. 7. Gas permeation property for pure Al_2O_3 with the different thicknesses (60, 100, 140, and 200 nm) and graded structures 140 nm thick.

structures was improved by up to a factor of 3 (i.e., 0.059 g m^{-2} day^{-1} for the sandwich graded layer) over the reference (see Fig. 7). The gas barrier properties follow a trend similar to that of the mechanical properties, with graded structures better than pure layers. The enhanced gas barrier performance is therefore attributed to the synergetic effect between better stress balance of the graded structure and the high local homogeneity of the film.

Also of interest is the effect of the Al–O–Si bonds in the graded film on its barrier properties. These bonds contribute to the enhanced mechanical properties, but it is unclear whether they are also directly responsible for the improvement in barrier properties. To settle this complicated question, an indirect method was used which measures the optical properties of the layer. It was found that the refractive index of the mixed films (i.e., non-graded structure) can be used to estimate the gas barrier behavior, since the optical properties depend on the polarizability of the oxides and the packing density of the films [37]. In other words, the refractive index increases when the polarizability and the density of the barrier layer increase, resulting in a better gas barrier. The refractive index of inorganic layers made up of a homogeneous mixture of Al_2O_3 and SiO_2 was measured as a function of the atomic concentration of Al_2O_3, from 0% to 100%, and a linear increase was observed (Fig. 8a). These results reflect the superior barrier properties of Al_2O_3 over SiO_2, but the linear increase indicates that the Al–O–Si bonds did not contribute directly to the barrier properties. Fig. 8b confirms that the barrier properties of the Al_2O_3/SiO_2 mixtures, without any gradient, lay between those of the two pure materials. These results confirm the superiority of using a graded architecture for improving the barrier properties, rather than a homogeneous mixture of two components, given the same average composition. Consequently, even if the mechanical properties of the homogeneous mixture were significantly improved over pure Al_2O_3, the mixture did not maintain the excellent barrier properties of pure Al_2O_3 layers. In contrast, the graded sandwich architecture with a pure Al_2O_3 zone preserved in the core of the film combined superior mechanical performance with enhancing the barrier properties. The progressive concentration change to SiO_2 at the top and the bottom part of the layer preserved the overall mechanical properties of the layer, and protected the Al_2O_3-rich zone from damage.

4. Conclusions

The graded approach used in this study for the deposition of inorganic layers demonstrated clear potential for the fabrication of inorganic oxide thin films with superior mechanical stability (i.e., enhanced toughness) and without losing optical transparency. Through the power control of the co-sputtering unit, the structural design of the thin film could easily be tailored on the nanometer scale. The absence of interfaces and the alternating bonding structures between different materials allowed the production of thin films with a chemical composition that was finely adjusted throughout the thickness. Furthermore, the internal chemical and mechanical balancing across the thickness could provide improved mechanical properties of inorganic thin films. Materials, blending ratios and architectures different from those used in the present study should give rise to further improvement in the mechanical and barrier performance of single inorganic layers. This approach makes

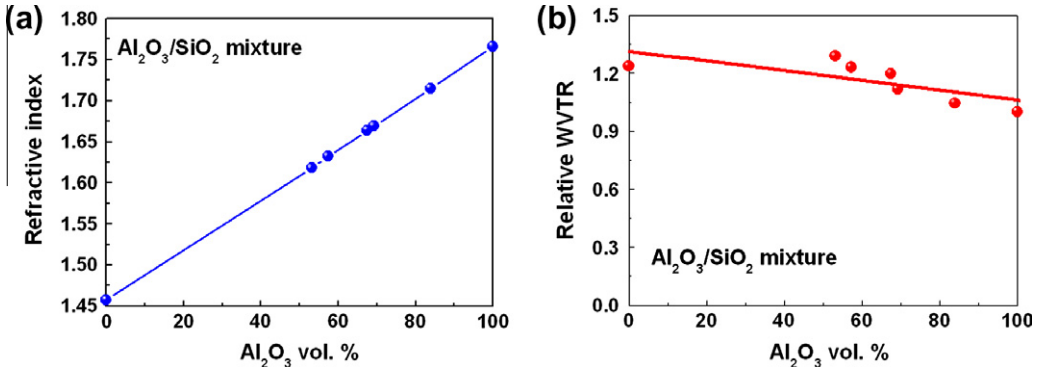

Fig. 8. Relationship between optical and permeation properties: (a) refractive index of simple mixtures of Al_2O_3 and SiO_2, where 0% in the x-axis denotes pure SiO_2 and (b) relative WVTR for the mixtures used in (a).

it possible to choose the material composition at critical points of the inorganic thin film so as to optimize performance. Critical points include the composition at the interface with the polymer substrate, to improve interfacial adhesion; the composition at the top surface to avoid crack initiation or control the density of defects at the surface; and the composition in the core, to give better balance of stresses within the film.

Acknowledgement

This work was supported financially by Samsung Advanced Institute of Technology.

References

[1] Mann S, Ozin GA. Nature 1996;382:313.
[2] Li J, Han Y. Langmuir 2006;22:1885.
[3] Deepa M, Srivastava AK, Lauterbach S, Govind, Shivaprasad SM, Sood KN. Acta Mater 2007;55:6095.
[4] Kim DW, Lee DY, Lee HS, Lee WH, Kim YH, Han JI, et al. Adv Mater 2007;19:678.
[5] Liu F, Li X, Zhao Q, Hou Y, Quan X, Chen G. Acta Mater 2009;57:2684.
[6] Placencia D, Wang W, Shallcross RC, Nebesny KW, Brumbach M, Armstrong NR. Adv Funct Mater 2009;19:1913.
[7] Lee YG, Choi Y-H, Kee IS, Shim HS, Jin Y, Lee S, et al. Org Electron 2009;10:1352.
[8] Choi Y-H, Lee YG, Lee K-H, Bulliard X, Lee S, Choi D, et al. Scripta Mater 2010;62:447.
[9] Choi Y, Choi D, Lee LP. Adv Mater 2010;22:1754.
[10] Choi D, Choi Y, Hong S, Kang T, Lee LP. Small 2010;6:1741.
[11] Lu N, Suo Z, Vlassak JJ. Acta Mater 2010;58:1679.
[12] Choi M-Y, Choi D, Jin M-J, Kim IS, Kim S-Y, Choi J-Y, et al. Adv Mater 2009;21:2185.
[13] Choi D, Choi M-Y, Shin HJ, Yoon SM, Seo JS, Lee S, et al. J Phys Chem C 2010;114:1379.
[14] Kim T-H, Choi WM, Kim D-H, Meitl MA, Menard E, Jiang H, et al. Adv Mater 2008;20:2171.
[15] Henry BM, Erlat AG, McGuigan A, Grovenor CRM, Briggs GAD, Tsukahara Y, et al. Thin Solid Films 2001;382:194.
[16] Mandlik P, Gartside J, Han L, Cheng I-C, Wagner S, Silvernail JA, et al. Appl Phys Lett 2008;92:103309.
[17] Carcia PF, McLean RS, Reilly MH, Groner MD, George SM. Appl Phys Lett 2006;89:031915.
[18] Muller DA, Nakagawa N, Ohtomo A, Grazul JL, Hwang HY. Nature 2004;430:657.
[19] Kwak S, Jun J, Jung E-S. Langmuir 2009;25:8051.
[20] Mattsson J, Forrest JA, Borjesson L. Phys Rev E 2000;62:5187.
[21] Nardin C, Winterhalter M, Meier W. Langmuir 2000;16:7708.
[22] Mallwitz F, Goedel WA. Angew Chem Int Ed 2001;40:2645.
[23] Jitcharoen J, Padture NP, Giannakopoulos AE, Suresh S. J Am Ceram Soc 1998;81:2301.
[24] Yin HM, Sun LZ, Paulino GH. Acta Mater 2004;52:3535.
[25] Cannillo V, Montorsi M, Siligardi C, Sola A, Portu Gd, Micele L, et al. J Eur Ceram Soc 2006;26:1411.
[26] Frank FC, Lawn BR. Proc R Soc London A 1967;299:291.
[27] Leterrier Y, Médico L, Demarco F, Månson J-AE, Escola-Figuera M, Kharrazi-Olsson M, et al. Thin Solid Films 2004;460:156.
[28] Leterrier Y, Fischer C, Médico L, Demarco F, Månson J-AE, Bouten P, DeGoede J, Nairn JA. In: 46th Annual technical conference proceedings of the society of vacuum coaters; 2003, vol. 505. p. 856.
[29] Bieder A, Gondoin V, Leterrier Y, Tornare G, PRv Rohr, Månson J-AE. Thin Solid Films 2007;515:5430.
[30] Leterrier Y, Boogh L, Andersons J, Månson J-AE. J Polym Sci Part B 1997;35:1449.
[31] Leterrier Y, Andersons J, Pitton Y, Månson J-AE. J Polym Sci Part B 1997;35:1463.
[32] Beuth JL. Int J Sol Struct 1992;29:1657.
[33] Andersons J, Modniks J, Leterrier Y, Tornare G, Dumont P, Månson J-AE. Theor Appl Fract Mech 2008;49:151.
[34] Schwarzer N. Surf Coat Technol 2000;133/134:397.
[35] Kelly A, Tyson WR. J Mech Phys Sol 1965;13:329.
[36] Howells DG, Henry BM, Leterrier Y, Månson J-AE, Madocks J, Assender HE. Surf Coat Tech 2008;202:3529.
[37] Koo WH, Jeong SM, Choi SH, Baik HK, Lee SM, Lee SJ. J Phys Chem B 2004;108:18884.